

# Influence and information in a collective of self-propelled particles

Jiahuan Pang,<sup>1</sup> and Wendong Wang<sup>1,\*</sup>

<sup>1</sup> Shanghai Jiao Tong University, Shanghai 200240, China.

While information-theoretic quantities, such as transfer entropy, have been widely adopted to infer causal relationships in collective systems, a critical gap exists: the absence of quantitative evidence directly linking information-theoretic quantities to a physically defined influence. This letter addresses this gap by proposing a modified Vicsek model that enables the calculation of a physically interpretable influence grounded in the angular interactions between particles. Averaged pairwise influences can serve as new order parameters to indicate collective phase transitions. We reveal quantitative relations between information, represented by transfer entropy, and average influence in pairwise and collective interactions. We test three typical methods of partial information decomposition and find that the method based on intrinsic mutual information gives the most appropriate interpretation. Overall, this work provides a model system for quantitative studies of influence and information in complex systems.

*Introduction*—Natural and artificial collective systems, such as bird flocks, colloidal swarms, and robot collectives, self-organize via local interactions to perform emergent behaviors and functions [1–7]. To analyze the local interactions, one approach is to use information-theoretic quantities to infer causal relations or degrees of influence from time series of observations [8]. The recent work by Sattari et. al. uses time-delayed mutual information, transfer entropy (TE) [9], and intrinsic information, shared information, and synergistic information obtained from partial information decomposition (PID) to infer influences between individuals in pairwise interactions in an augmented Vicsek model [7]. Their approach, however, lacks a direct measure of influence to verify the inferred causal relations or degrees of influence.

Here we modify the Vicsek model to allow direct calculations of orientational influences in pairwise interactions. We show that suitable averages of pairwise influences can indicate the phase transition of the modified Vicsek model. We analyze quantitatively the relations between TE and influence to reveal the dual effects of noise. We further devise a way to aggregate a particle’s neighbors’ orientation data and use the aggregated data to show the effectiveness of various information-theoretic quantities in identifying the phase transition. Among the many PID methods [10–18] (see SI section S1 and Fig. S1 for an overview), we select average minimum information (AMI) method [10], intrinsic mutual information (IMI) method [15], and synergistic unique-redundant decomposition of causality (SURD) method [16] to decipher the nature of orientational influence. We envision that our work will not only provide a model system to analyze information and influence, but also provide a way to compare the effectiveness of various

information-theoretic tools in analyzing complex systems.

*Modification of the Vicsek model*—In the Vicsek model [19–22], each particle adjusts its direction to align with the average direction of the velocities of its neighboring particles. We express the direction  $\theta_i(t + \Delta t)$  of particle  $i$  at time  $t + \Delta t$ , as the angle of the sum of its direction  $\theta_i(t)$  at  $t$ , the angle change  $A_i$  induced by its neighbors, and noise  $\beta_i$ :

$$\theta_i(t + \Delta t) = F(\theta_i(t) + A_i(t) + \beta_i(t)), \quad (1)$$

where

$$A_i(t) = \sum_j^N A_{j \rightarrow i}(t) \quad (2)$$

and

$$A_{j \rightarrow i}(t) = \frac{w_{j \rightarrow i} F(\theta_j(t) - \theta_i(t)) s_{ij}(t)}{\sum_j w_{j \rightarrow i} s_{ij}(t)}. \quad (3)$$

$\beta_i(t)$  represents the noise uniformly distributed in  $[-\eta/2, \eta/2]$ , and  $\eta \in [0, 2\pi]$  is the strength of noise.  $\Delta t$  is the discrete time step;  $N$  is the number of particles;  $w_{j \rightarrow i}$  is the interaction weight particle  $j$  exerts on particle  $i$ .  $F(\cdot)$  is the function that constrains the value of an angle to be within  $(-\pi, \pi]$ ,

$$F(x) = \begin{cases} x \% 2\pi, & x \% 2\pi \leq \pi \\ x \% 2\pi - 2\pi, & x \% 2\pi > \pi \end{cases} \quad (4)$$

where  $\%$  is the modulo operator.  $s_{ij}(t)$  indicates whether two particles are neighbors: it can be written as a Heaviside function  $H(R - |\mathbf{r}_j(t) - \mathbf{r}_i(t)|)$ , which is one or zero when the distance between two particles is equal and smaller or larger than the interaction cutoff radius  $R$ , respectively.

This modification of Vicsek model allows us to define  $A_{j \rightarrow i}(t)$  as the **influence** exerted by particle  $j$  on particle  $i$  at time  $t$ . Because  $A_{j \rightarrow i}(t)$  is weighted by

\*Corresponding author: wendong.wang@sjtu.edu.cn

pairwise interaction strength  $w_{j \rightarrow i}$  and normalized by the total weights of all neighboring particles, the sum of  $A_{j \rightarrow i}(t)$  over  $j$ ,  $A_i(t)$ , is in fact the weighted average influence by all neighboring particles on particle  $i$  at time  $t$ . Using Eq. (2) and Eq. (3), we could directly calculate the influence received by individual particles. This direct calculation is unfeasible in the original Vicsek model because the original Vicsek model uses a combination of nonlinear trigonometric functions to extract the average direction of particles in a local neighborhood. Further details about the simulations are in the SI section S2.

*Phase transition of the modified Vicsek model*—The modified Vicsek model preserves the order-disorder phase transition of the original Vicsek model. To demonstrate this essential characteristic, we set all pairwise interaction weights  $w_{j \rightarrow i}$  to unity and perform simulations by varying the number of particles  $N$ , the interaction cutoff radius  $R$ , and the noise strength  $\eta$ . The order parameter of the original Vicsek model is the time average of the norms of mean velocities  $|\overline{v_a}|$ :

$$|\overline{v_a}| = \frac{1}{T} \sum_t (|v_a(t)|) = \frac{1}{T} \sum_t \left| \frac{1}{Nv} \sum_i v_i(t) \right|, \quad (5)$$

where  $T$  denotes the total number of time steps; the overbar represents the time average. Fig. 1(a) shows that  $|\overline{v_a}|$  decreases as the noise strength  $\eta$  increases, similar to the behavior of the original Vicsek model [19]. The transition occurs at  $\eta \approx \pi$ . In addition,  $|\overline{v_a}|$  increases as the particle density increases, as shown in Fig. S2, also similar to the original Vicsek model [19].

Based on our definition of influence, we introduce a new order parameter: the time average of the number average of the norms of neighbor-averaged influences:

$$\overline{\langle |A_R| \rangle_N} = \frac{1}{T} \sum_{t=1}^T \frac{1}{N} \sum_{i=1}^N \left| \sum_j A_{j \rightarrow i}(t) \right|, \quad (6)$$

where  $\langle \cdot \rangle_R$  represents averaging over neighbors within a radius of  $R$ ;  $\langle \cdot \rangle_N$  represents averaging over the number of particles  $N$ ; the overbar represents the time average. The specific combination of three averaging operations and one norm operation in the definition is one of 24 possible combinations. We have chosen  $\overline{\langle |A_R| \rangle_N}$  because it produces an inverted V-shape around the transition point [Fig. 1(b)], thereby allowing unambiguous identification of the transition point. There are three other unique combinations, but they are less effective in identifying phase transitions (see SI section S3 and Fig. S3). Note in Fig. 1(b) that plots of different particle numbers collapsed into one curve, in contrast to  $|\overline{v_a}|$  in Fig. 1(a).

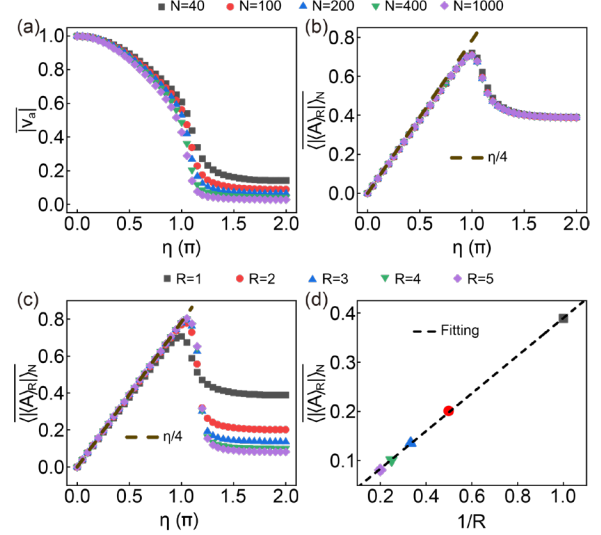


FIG. 1. (a) The time average of the absolute value of the average velocity  $|\overline{v_a}|$  versus the noise strength  $\eta$  for different number of particles  $N$  at a fixed density  $\rho = 4$  and a fixed neighborhood radius  $R = 1$ . (b) Influence-based order parameter  $\overline{\langle |A_R| \rangle_N}$  versus  $\eta$  for different  $N$  at  $\rho = 4$  and  $R = 1$ . The brown dashed line is plotted according to Eq. (7). (c)  $\overline{\langle |A_R| \rangle_N}$  versus  $\eta$  for five values of  $R$  at  $\rho = 4$  and  $N = 400$ . (d) The values of  $\overline{\langle |A_R| \rangle_N}$  at  $\eta = 2\pi$  versus  $1/R$ .

In the ordered states ( $\eta < \pi$ ), we derive the values of  $\overline{\langle |A_R| \rangle_N}$  as follows. We postulate that in an ordered state, the influences on one particle by all neighbors align the particle in the direction  $\theta_{order}$  at each time step:  $\theta_{order} = \theta_i(t) + A_i(t)$ . As a result,  $|A_i| = |\beta_i|$ . Because  $\beta_i$  is uniformly distributed in  $[-\eta/2, \eta/2]$ , its norm  $|\beta_i|$  is uniformly distributed in  $[0, \eta/2]$ . Therefore, the average of  $|\beta_i|$  is  $\eta/4$ :

$$\overline{\langle |A_R| \rangle_N} = E(|\beta_i|) \approx \frac{\eta}{4}, \quad \eta < \pi. \quad (7)$$

This analytical result, plotted as the dashed yellow line in Fig. 1(b), agrees well with the simulation results.

The asymptotic value of  $\overline{\langle |A_R| \rangle_N}$  at  $\eta = 2\pi$  can be seen as the expectation value of  $|A_i|$  over a normal distribution  $\mathcal{N}(0, \pi^2/3n)$ , where  $n = \pi R^2 \rho$  is the average number of neighbors. Hence, the expectation value  $E(|A_i|) = \sqrt{2/(3R^2 \rho)} \propto 1/R$  [Figs. 1(b)-(c)]. Further details are in SI Section S3.

*Influence and transfer entropy*—We begin our analysis of influence and information using a simple one-way interaction setup in a two-particle system [Fig. 2(a)]. In this setup, the interaction weight  $w_{I \rightarrow F}$  from an influencer  $I$  to a follower  $F$  is tunable, and the follower does not exert influence on the influencer, i.e.,  $w_{F \rightarrow I} = 0$ . The self-interaction weight of the follower  $w_{F \rightarrow F}$  was set to unity. The self-interaction weight of

the influence  $w_{I \rightarrow I}$  can take any nonzero values because  $A_{I \rightarrow I} = 0$ .

To quantify influence, we measure the time-averaged absolute influence that the influencer  $I$  exerts on the follower  $F$ :

$$\overline{|A_{I \rightarrow F}|} = \frac{1}{T} \sum_t |A_{I \rightarrow F}(t)|. \quad (8)$$

Fig. 2(b) shows the effect of noise strength  $\eta$  on  $\overline{|A_{I \rightarrow F}|}$  for five different values of  $w_{I \rightarrow F}$ , and Fig. 2(c) shows the effect of  $w_{I \rightarrow F}$  on  $\overline{|A_{I \rightarrow F}|}$  for five different  $\eta$ . The symbols are simulation results, and the curves are analytical results, calculated according to Eq. (9):

When  $0 \leq \eta \leq \pi$ ,

$$\overline{|A_{I \rightarrow F}|} = \frac{w_{I \rightarrow F}}{w_{I \rightarrow F} + w_{F \rightarrow F}} \times \frac{\eta}{3}. \quad (9a)$$

When  $\pi \leq \eta \leq 2\pi$ ,

$$\overline{|A_{I \rightarrow F}|} = \frac{w_{I \rightarrow F}}{w_{I \rightarrow F} + w_{F \rightarrow F}} \times \left( \frac{2\pi^3 - 6\pi^2\eta + 6\pi\eta^2 - \eta^3}{3\eta^2} \right). \quad (9b)$$

The derivations of the above analytical expressions are in SI section S4. Both the simulation and analytical results show that increasing weight  $w_{I \rightarrow F}$  and increasing noise strength  $\eta$  increase the influence  $\overline{|A_{I \rightarrow F}|}$ . The effect of weight  $w_{I \rightarrow F}$  fits the intuition that higher interaction weight leads to higher influence. The effect of noise strength can be understood intuitively as follows: higher noise strength leads to higher deviation of the follower from the influencer, which requires higher influence to align the follower to the influencer.

We compute TE from the joint probability distribution  $p(\theta_I(t), \theta_F(t), \theta_F(t + \Delta t))$ . The joint probability distribution was based on the set of triples  $(\theta_I(t), \theta_F(t), \theta_F(t + \Delta t))$  obtained from the entire duration of the simulations to get sufficient statistics. We measure the TE from  $\theta_I(t)$  to  $\theta_F(t + \Delta t)$  to investigate the information flow from the influencer to the follower. To provide an intuitive understanding of the results in Figs. 2(d)-(f), we highlight the dual effects of noise. The influence  $A_{I \rightarrow F}(t)$  is a function of two variables  $\theta_I(t)$  and  $\theta_F(t)$ , and it quantifies the angular adjustment the influencer imparts on the follower. Higher noise leads to larger difference between  $\theta_I(t)$  and  $\theta_F(t)$  and hence higher influence, which intuitively should increase TE. However, TE involves an additional variable  $\theta_F(t + \Delta t)$ , which not only depends on  $\theta_I(t)$ ,  $\theta_F(t)$  but also noise  $\beta_F(t)$ , so increasing the noise strength increases the relative importance of  $\beta_F(t)$  and leads to a decrease in TE. The transition of the balance between these two effects occurs at  $\eta \approx \pi$ : when  $\eta < \pi$ , increasing  $\eta$  increases both  $\overline{|A_{I \rightarrow F}|}$  and TE; when  $\eta > \pi$ , increasing  $\eta$

increases  $\overline{|A_{I \rightarrow F}|}$  but decreases TE. An example of this balance is shown in Fig. 2(d).

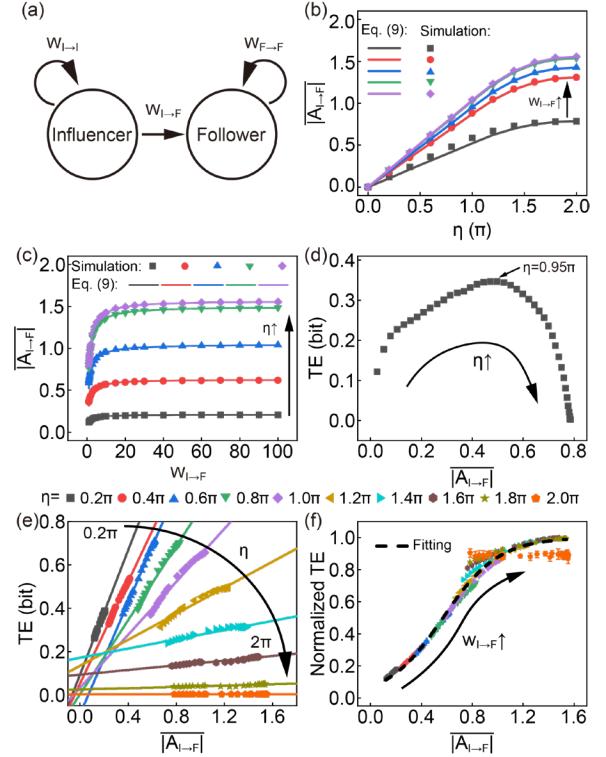


FIG. 2. (a) Diagram of one-way influence pairwise interaction. The arrows indicate the directions of influence. (b) Influence  $\overline{|A_{I \rightarrow F}|}$  versus  $\eta$  at  $w_{I \rightarrow F} = 1, 5, 10, 50$  and  $100$ . Symbols are simulation results. Lines are analytical results. (c) Influence  $\overline{|A_{I \rightarrow F}|}$  versus  $w_{I \rightarrow F}$  at  $\eta = 0.2\pi, 0.6\pi, 1.0\pi, 1.6\pi, 2.0\pi$ . Symbols are simulation results. Lines are analytical results. (d) TE versus  $\overline{|A_{I \rightarrow F}|}$  with  $w_{I \rightarrow F} = 1$  and  $\eta \in [0, 2\pi]$ . (e) TE versus  $\overline{|A_{I \rightarrow F}|}$ . Each color represents one noise strength. The weights vary from 1 to 100. Symbols of the same color represent different weights of the same noise strength. Lines are linear fittings. (f) Normalized TE versus  $\overline{|A_{I \rightarrow F}|}$ . The black dashed curve is fitted according to Boltzmann sigmoid function.

Fig. 2(d) shows the dependence of TE on  $\overline{|A_{I \rightarrow F}|}$  as  $\eta$  changes from 0 to  $2\pi$  at a fixed  $w_{I \rightarrow F} = 1$ . When  $\eta = 0.95\pi$ , TE has the maximum value of 0.347, and the corresponding  $\overline{|A_{I \rightarrow F}|}$  is 0.497. The existence of a maximum point on the curve is a direct manifestation of the dual effects of noise. Moreover, the value of  $\eta$  at the maximum TE in pairwise interaction and the values of  $\eta$  at the collective phase transitions [Figs. 1 (b)-(c)] are very close, which suggests that maximum information transfer occurs near the phase transitions. This result agrees with the hypothesis that a collective's ability to process information is maximum near its phase transition, or critical point [21,22].

Fig. 2(e) shows that TE and  $\overline{|A_{I \rightarrow F}|}$  as functions of  $w_{I \rightarrow F}$  and  $\eta$ . The noise strength  $\eta$  varies between  $0.2\pi$  and  $2\pi$ . As  $w_{I \rightarrow F}$  increases from 1 to 100, TE and  $\overline{|A_{I \rightarrow F}|}$  follow roughly a linear relation at a fixed  $\eta$ . We can infer the balance of dual effects of noise from the the  $R^2$  (coefficient of determination) values of the linear fitting. When  $\eta$  increases from  $0.2\pi$  to  $0.8\pi$ , the  $R^2$  values of the linear fitting are above 0.99 (Fig. S4), indicating a high degree of correlation between influence and TE. Hence, the relative importance of noise in TE is small. As  $\eta$  further increases from  $\pi$  to  $2\pi$ , the  $R^2$  values of the linear fitting decreases from  $\sim 0.99$  to  $\sim 0.04$ , indicating a decrease in the correlation between TE and influence. Hence, the relative importance of noise increases. In particular, at  $\eta = 2\pi$ , the  $R^2$  value is  $\sim 0.04$ , and TE is near zero. It indicates that the noise overwhelms any information the influencer gives to the follower.

To gain further insights, we normalize TE by the mutual information  $I(\theta_I(t), \theta_F(t); \theta_F(t + \Delta t))$  [16].  $I(\theta_I(t), \theta_F(t); \theta_F(t + \Delta t))$  represents the information given by both the influencer's present,  $\theta_I(t)$ , and the follower's present,  $\theta_F(t)$ , to the follower's future,  $\theta_F(t + \Delta t)$  (Fig. S5), whereas TE represents the information given by  $\theta_I(t)$  to  $\theta_F(t + \Delta t)$ . Therefore, the normalized TE represents the ratio between the information given by the influencer and the information given by both the influencer and the follower. Fig. 2(f) shows that the data points of normalized TE versus  $\overline{|A_{I \rightarrow F}|}$  for various noise strengths and weights collapse onto one curve, except for the case  $\eta = 2.0\pi$  because of the complete dominance of noise. This curve can be fitted with the Boltzmann sigmoid function:

$$\text{normalized TE} = \frac{\exp(\overline{|A_{I \rightarrow F}|}/k)}{\exp(\overline{|A_{I \rightarrow F}|}/k) + \exp(a/k)} \quad (10)$$

with fitting parameters  $a = 0.570 \pm 0.002$  and  $k = 0.218 \pm 0.002$ . The term  $\exp(\overline{|A_{I \rightarrow F}|}/k)$  represents the Boltzmann weight of the influence from the influencer to the follower, and the term  $\exp(a/k)$  represents the Boltzmann weight of an effective self-influence of the follower. This effective self-influence cannot be calculated using Eq. (3) because it will give zero value. The value of  $k$  dictates the shape of the curve: when normalized TE is 0.5 (i.e.  $\overline{|A_{I \rightarrow F}|} = a$ ), the slope of the curve reaches a maximum value of  $1/(4k)$ . The fact that the fitted curve is sigmoidal indicates a monotonous increase of normalized TE as  $\overline{|A_{I \rightarrow F}|}$  increases. This increase is monotonous because when we only consider  $\theta_I(t)$  and  $\theta_F(t)$ , influencer's relative importance increases with increasing  $\overline{|A_{I \rightarrow F}|}$ .

*Information and phase transition*—Because influence can indicate phase transitions (Fig. 1) and because information and influence are quantitatively related (Fig. 2), we ask the question: how to infer phase transitions from information? The technical difficulty in addressing this question directly using information-theoretical quantities based on multiple variables is that the complexity of calculation increases very quickly as the number of variables increases [10,16]. To circumvent this difficulty, we devise the following method to treat all neighbors as one entity. First, we collect triples of angular orientations  $(\theta_j(t), \theta_i(t), \theta_i(t + \Delta t))$  for all neighboring pairs  $(i, j)$  over the entire duration of a simulation; then we consider  $\theta_j(t)$ 's of all the neighbors of particle  $i$  as a single variable  $\theta_{nbs}(t)$  and obtain the aggregated set of triples  $(\theta_{nbs}(t), \theta_i(t), \theta_i(t + \Delta t))$  for each particle  $i$ ; next, we construct the joint probability distribution  $p(\theta_{nbs}(t), \theta_i(t), \theta_i(t + \Delta t))$  and compute a single value of an information-theoretic quantity, which we interpret as the information that the environment provides to the particle  $i$ ; finally, we average the values of the information-theoretic quantity over particles. We find that the normalized TE from  $\theta_{nbs}(t)$  to  $\theta_i(t + \Delta t)$  and its decompositions can indicate phase transitions (Fig. 3 and Figs. S6-S12).

Fig. 3(a) shows that the curves of the normalized TE versus the noise strength  $\eta$  have a cusp point at  $\eta \approx \pi$  and that the positions of the cusp points do not depend on the number of particles. Fig. 3(b) shows that the positions of the cusp points shift to slightly higher values of normalized TE and  $\eta$  as the neighborhood radius  $R$  increases: when  $R = 1, 2$ , the cusp points are at  $\eta_c = 0.95\pi$  and  $\pi$ , respectively; when  $R \geq 3$ ,  $\eta_c = 1.05\pi$ . The sudden rise in normalized TE near  $\eta = 2\pi$  diminishes as  $R$  increases, which suggests that this rise is due to insufficient statistics and is not indicative of another phase transition.

The curves' inverted V-shapes in Fig. 3(b) are similar to the curves of averaged influence versus noise in Fig. 1(c). This similarity prompts us to plot normalized TE versus averaged influence directly. Fig. 3(c) shows an example of the normalized TE versus averaged influence plots for  $R = 5$ . The curve has two regions with the transition occurs at  $\eta = 1.05\pi$ . These two regions can be fitted with two power laws separately: the powers are 2.4 and 3.8 for the first and the second regions, respectively. The values of the powers are similar for  $R = 3, 4$  (Fig. S6). These separate regions and power laws highlight again the dual effects of noise in the collective behaviors: in the low noise region, increasing noise strength increases both normalized TE and averaged influence, whereas

in the high noise region, increasing noise strength decreases both normalized TE and averaged influence.

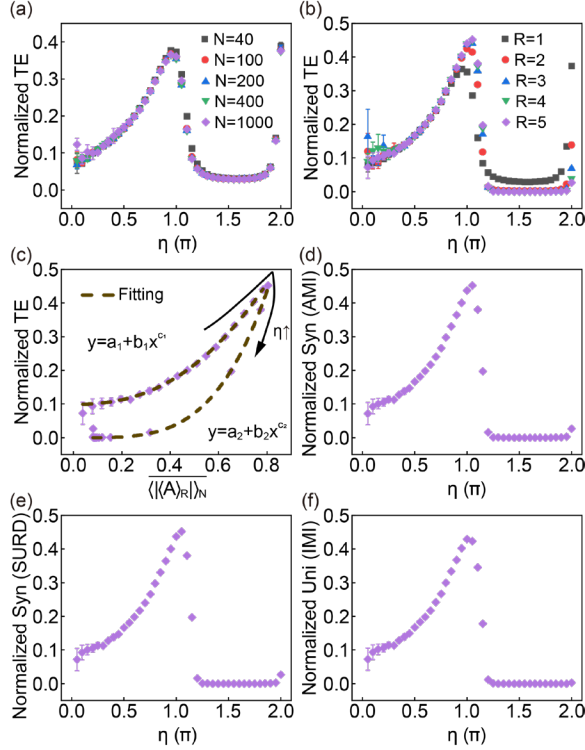


FIG. 3. Comparison among different information-theoretic quantities in indicating the phase transition of the modified Vicsek model for a fixed density  $\rho = 4$ . (a) Normalized TE versus noise  $\eta$  for  $R = 1$ . (b) Normalized TE versus  $\eta$  for five values of  $R$  at  $\rho = 4$  and  $N = 400$ . (c) Normalized TE versus  $\langle\langle A \rangle_R\rangle_N$  at  $N = 400$  and  $R = 5$ . The values of the fitting parameters are  $a_1 = 0.099 \pm 0.002$ ,  $b_1 = 0.611 \pm 0.004$ ,  $c_1 = 2.375 \pm 0.036$ ,  $a_2 = 0$ ,  $b_2 = 1.018 \pm 0.118$ , and  $c_2 = 3.803 \pm 0.291$ . (d) Normalized synergistic information based on AMI method versus  $\eta$  at  $N = 400$  and  $R = 5$ . (e) Normalized synergistic information based on SURD method versus  $\eta$  at  $N = 400$  and  $R = 5$ . (f) Normalized unique (intrinsic) information based on IMI method versus  $\eta$  at  $N = 400$  and  $R = 5$ .

To gain further insights about the relation between influence and information, we calculate the decomposed information based on AMI, SURD, and IMI methods [Figs. 3(d)-(f) and Figs. S7-S12]. Our most notable finding is that AMI and SURD attribute most of the TE to synergistic information, whereas IMI attributes most of the TE to unique information. This difference in attribution compelled us to examine the nature of influence in our modified Vicsek model.

Because  $A_{j \rightarrow i}(t)$  represents the angular change of the particle  $i$  caused by the particle  $j$  and comes only from the particle  $j$  at time  $t$ , and because the noise strengths of different particles are independent random

variables, we think that the influence  $\overline{\langle\langle A \rangle_R\rangle_N}$  should reflect unique information. Therefore, the results in Fig. 3 support IMI as the more appropriate PID method. This conclusion is consistent with the previous findings that AMI overestimates synergistic information [11,23]. SURD and AMI share part of their theoretical construction, which is the concept of specific information [24], so it is likely that SURD also overestimates the synergistic information.

*Conclusion and discussion*—In conclusion, we have proposed a modified Vicsek model that allows us to define and calculate pairwise influence directly. The average of pairwise influences  $\overline{\langle\langle A \rangle_R\rangle_N}$  can serve as an effective new order parameter to indicate phase transitions. In pairwise interactions, TE and normalized TE show linear and sigmoidal relations with the influence  $|A_{I \rightarrow F}|$ , respectively. In collective interactions, by treating all neighbors  $\theta_j(t)$ 's as one entity  $\theta_{nbs}(t)$ , we found that normalized TE from  $\theta_{nbs}(t)$  to  $\theta_i(t + \Delta t)$  show an inverted V-shape near the phase transitions, similar to the behaviors of the average influence  $\overline{\langle\langle A \rangle_R\rangle_N}$  and that power law relations exist between the normalized TE and  $\overline{\langle\langle A \rangle_R\rangle_N}$ . Lastly, by analyzing the decomposed information based on three representative PID methods, we have found that our influence more closely reflects unique information and hence lends support to IMI as the appropriate PID method.

This work takes a further step beyond Sulimon's work [7] by defining a physically interpretable influence and by investigating both pairwise interactions and collective interactions. It provides a model with a direct measure of influence and will serve as a platform for analyzing collective information processing near critical points and for examining information-theoretic quantities for causal inference in complex systems.

Future efforts will examine the nature of the phase transition in the modified Vicsek model in large systems [20,21] and explore the generalization of the definition of influence in other systems. In addition, we will explore experimental systems in which both influence and information-theoretic quantities can be directly calculated or measured.

*Acknowledgement*—This work was supported by the National Natural Science Foundation of China (project number 22175115), the Science and Technology Commission of Shanghai Municipality (project number 23ZR1433700), and the start-up fund of SJTU.

[1] P. Ball, *Nature's Patterns : A Tapestry in Three Parts*, Published in paperback (Oxford Univ. Press, Oxford, 2009).

- [2] T. Vicsek and A. Zafeiris, Collective motion, *Phys. Rep.* **517**, 71 (2012).
- [3] H. Yu, Y. Fu, X. Zhang, L. Chen, D. Qi, J. Shi, and W. Wang, Programmable active matter across scales, *Program. Mater.* **1**, e7 (2023).
- [4] M. Nagy, Z. Ákos, D. Biro, and T. Vicsek, Hierarchical group dynamics in pigeon flocks, *Nature* **464**, 890 (2010).
- [5] S. Butail, V. Mwaffo, and M. Porfiri, Model-free information-theoretic approach to infer leadership in pairs of zebrafish, *Phys. Rev. E* **93**, 042411 (2016).
- [6] W. Wang et al., Order and information in the patterns of spinning magnetic micro-disks at the air-water interface, *Sci. Adv.* **8**, eabk0685 (2022).
- [7] S. Sattari, U. S. Basak, R. G. James, L. W. Perrin, J. P. Crutchfield, and T. Komatsuzaki, Modes of information flow in collective cohesion, *Sci. Adv.* **8**, eabj1720 (2022).
- [8] K. Hlaváčková-Schindler, M. Paluš, M. Vejmelka, and J. Bhattacharya, Causality detection based on information-theoretic approaches in time series analysis, *Phys. Rep.* **441**, 1 (2007).
- [9] T. Schreiber, Measuring Information Transfer, *Phys. Rev. Lett.* **85**, 461 (2000).
- [10] P. L. Williams and R. D. Beer, *Nonnegative Decomposition of Multivariate Information*, arXiv:1004.2515.
- [11] M. Harder, C. Salge, and D. Polani, Bivariate measure of redundant information, *Phys. Rev. E* **87**, 012130 (2013).
- [12] N. Bertschinger, J. Rauh, E. Olbrich, J. Jost, and N. Ay, Quantifying Unique Information, *Entropy* **16**, 4 (2014).
- [13] J. Rauh, Secret Sharing and Shared Information, *Entropy* **19**, 11 (2017).
- [14] R. A. A. Ince, Measuring Multivariate Redundant Information with Pointwise Common Change in Surprisal, *Entropy* **19**, 7 (2017).
- [15] R. G. James, B. D. M. Ayala, B. Zakirov, and J. P. Crutchfield, *Modes of Information Flow*, arXiv:1808.06723.
- [16] Á. Martínez-Sánchez, G. Arranz, and A. Lozano-Durán, Decomposing causality into its synergistic, unique, and redundant components, *Nat. Commun.* **15**, 9296 (2024).
- [17] R. G. James, J. Emenheiser, and J. P. Crutchfield, Unique information via dependency constraints, *J. Phys. Math. Theor.* **52**, 014002 (2018).
- [18] R. G. James, J. Emenheiser, and J. P. Crutchfield, Unique Information and Secret Key Agreement, *Entropy* **21**, 1 (2019).
- [19] T. Vicsek, A. Czirók, E. Ben-Jacob, I. Cohen, and O. Shochet, Novel Type of Phase Transition in a System of Self-Driven Particles, *Phys. Rev. Lett.* **75**, 1226 (1995).
- [20] G. Grégoire and H. Chaté, Onset of Collective and Cohesive Motion, *Phys. Rev. Lett.* **92**, 025702 (2004).
- [21] H. Chaté, F. Ginelli, G. Grégoire, and F. Raynaud, Collective motion of self-propelled particles interacting without cohesion, *Phys. Rev. E* **77**, 046113 (2008).
- [22] F. Ginelli, The Physics of the Vicsek model, *Eur. Phys. J. Spec. Top.* **225**, 2099 (2016).
- [23] T. Mora and W. Bialek, Are Biological Systems Poised at Criticality?, *J. Stat. Phys.* **144**, 268 (2011).
- [24] M. A. Muñoz, *Colloquium* : Criticality and dynamical scaling in living systems, *Rev. Mod. Phys.* **90**, 031001 (2018).
- [25] V. Griffith and C. Koch, *Quantifying Synergistic Mutual Information*, arXiv:1205.4265.
- [26] M. R. Deweese and M. Meister, How to measure the information gained from one symbol, *Netw. Comput. Neural Syst.* **10**, 325 (1999).

## **SUPPLEMENTARY INFORMATION.**

### **Influence and information in a collective of self-propelled agents**

Jiahuan Pang,<sup>1</sup> and Wendong Wang<sup>1,\*</sup>

<sup>1</sup> Shanghai Jiao Tong University, Shanghai 200240, China.

**This PDF file includes:**

Sections S1 to S5

Figures S1 to S12

SI Reference

## Table of contents

<b>S1. Information-theoretic quantities</b> .....	3
<b>S1.1. Time-delayed mutual information</b> .....	3
<b>S1.2. Transfer entropy</b> .....	3
<b>S1.3. Partial information decomposition method</b> .....	3
<b>S2. Simulation setup</b> .....	5
<b>S2.1 Phase transition with identical influence</b> .....	5
<b>S2.2 Pairwise interactions with one-way influence</b> .....	5
<b>S3. Phase transition and influences</b> .....	6
<b>S4. Influence and information in pairwise interaction</b> .....	9
<b>S5. Computation of information-theoretic quantities</b> .....	11
<b>Supplementary figures</b> .....	12
<b>SI Reference</b> .....	24

## S1. Information-theoretic quantities

This section gives a concise overview of the information-theoretic quantities commonly employed to quantify influence in complex systems.

### S1.1. Time-delayed mutual information

Consider two stationary random processes  $X = (\dots, x(t - \Delta t), x(t), x(t + \Delta t), \dots)$  and  $Y = (\dots, y(t - \Delta t), y(t), y(t + \Delta t), \dots)$  where  $t$  represents the time instants and  $\Delta t$  represents the discrete time step. The probability mass function  $p(x(t))$  represents the probability that  $X$  takes the value  $x(t)$ , and  $p(y(t))$  represents the probability that  $Y$  takes the value of  $y(t)$ . The mutual information between  $X$  and  $Y$ , denoted as  $I(X; Y)$ , quantifies the amount of information shared between the two processes and is defined as:

$$I(X; Y) = \sum_{x(t)} \sum_{y(t)} p(x(t), y(t)) \log \frac{p(x(t), y(t))}{p(x(t))p(y(t))}. \quad (1)$$

Historically, mutual information has been used to measure the causal influence of variable  $X$  on variable  $Y$ . However, since dynamic causal influence cannot occur instantaneously, TDMI was introduced to account for the time delay  $\Delta t$ , between the two processes. Incorporating a time delay  $\Delta t$  allows quantifying the dependency between two time series at different time points and figures the directionality. TDMI is defined as:

$$I(X(t); Y(t + \Delta t)) = \sum_{x(t)} \sum_{y(t+\tau)} p(x(t), y(t + \Delta t)) \log \frac{p(x(t), y(t + \Delta t))}{p(x(t))p(y(t + \Delta t))}.$$

The value of TDMI, measured in bits, indicates the extent to which  $Y$  is influenced by  $X$  after a time delay  $\tau$ .

### S1.2. Transfer entropy

However, TDMI failed to distinguish between actually exchanged information and shared information resulting from common history and input signals [1]. Specifically, TDMI ignores the present state of  $Y$ , which can lead to misleading conclusions about causal influence. To address this issue, Schreiber proposed TE, which conditions on the present state of  $Y$  to exclude shared information with  $X$ . TE is defined as:

$$I(X(t); Y(t + \Delta t) | Y(t)) = \sum_{x(t), y(t), y(t+\Delta t)} p(x(t), y(t), y(t + \Delta t)) \log \frac{p(x(t), y(t + \Delta t) | y(t))}{p(x(t) | y(t))p(y(t + \Delta t) | y(t))}.$$

TE has since become one of the standard measures for quantifying causal influence and is widely used across various fields [1–5].

### S1.3. Partial information decomposition method

Although TE has yielded many remarkable results in a wide range of applications, it has been demonstrated that TE fails to distinguish the intrinsic causal influence from the synergistic influence [6]. This limitation arises because the conditioning operation in TE may induce additional information, complicating the interpretation of causal relationships.

Consider two processes  $X$  and  $Y$ , assumed to be Markov processes. When analyzing how  $X$  influences  $Y$ , we can identify four distinct causal relationships:

1. Unique (Intrinsic) influence  $X(t)$  gives to  $Y(t + \Delta t)$  which represents the causal effect on  $Y(t + \Delta t)$  that arises ambiguously from  $X(t)$ .

2. Unique (Intrinsic) influence from  $Y(t)$  to  $Y(t + \Delta t)$ .
3. Redundant (Shared) influence from  $X(t)$  and  $Y(t)$  to  $Y(t + \Delta t)$ . This represents the influence on  $Y(t + \Delta t)$  that is redundantly provided by both  $X(t)$  and  $Y(t)$ .
4. Synergistic influence from  $X(t)$  and  $Y(t)$  to  $Y(t + \Delta t)$ . This represents the influence on  $Y(t + \Delta t)$  that emerges when  $X(t)$  and  $Y(t)$  are considered together, surpassing the combined effect of their individual influences.

As previously mentioned, TDMI failed to distinguish intrinsic influence from shared influence, while TE failed to distinguish intrinsic information from synergistic influence. To address these limitations, the partial information decomposition (PID) method has been proposed to differentiate among different modes of information, thereby identifying distinct modes of causal influence. Specifically, the PID method decomposes the total information between  $(X(t), Y(t))$  and  $Y(t + \Delta t)$ , denoted as  $I(X(t), Y(t); Y(t + \Delta t))$ , into the four distinct modes of information [Fig. S1].

$$\begin{aligned}
I(X(t), Y(t); Y(t + \Delta t)) &= Uni(X(t) \rightarrow Y(t + \Delta t)) \\
&\quad + Uni(Y(t) \rightarrow Y(t + \Delta t)) \\
&\quad + Red(X(t), Y(t) \rightarrow Y(t + \Delta t)) \\
&\quad + Syn(X(t), Y(t) \rightarrow Y(t + \Delta t)),
\end{aligned} \tag{1}$$

where  $Uni(X(t) \rightarrow Y(t + \Delta t))$  represents the unique information from  $X(t)$  to  $Y(t + \Delta t)$ ,  $Red(X(t), Y(t) \rightarrow Y(t + \Delta t))$  indicates the redundant information from  $X(t)$  and  $Y(t)$  to  $Y(t + \Delta t)$ , and  $Syn(X(t), Y(t) \rightarrow Y(t + \Delta t))$  represents the synergistic information from  $X(t)$  and  $Y(t)$  to  $Y(t + \Delta t)$ . Using PID, TDMI and TE can be expressed as

$$I(X(t); Y(t + \Delta t)) = Uni(X(t) \rightarrow Y(t + \Delta t)) + Red(X(t), Y(t) \rightarrow Y(t + \Delta t)), \tag{2}$$

and

$$I(X(t); Y(t + \Delta t) | Y(t)) = Uni(X(t) \rightarrow Y(t + \Delta t)) + Syn(X(t), Y(t) \rightarrow Y(t + \Delta t)). \tag{3}$$

This provides a more detailed representation of the information flow and causal interactions, allowing a more precise quantification of the different types of influence. With 3 equations, Eq. (1)-(3), and 4 types of information, one can complete the decomposition by measuring one of the four [6–15].

## S2. Simulation setup

The parameters of our simulations include the number of particles  $N$ , the size  $L$  of the simulation domain, the noise's strength  $\eta$ , the neighborhood's cutoff radius  $R$ , the particle speed  $v$ , the total time steps  $T$ , the time step size  $\Delta t$ , and pairwise interaction weight  $w_{i \rightarrow j}$ . For each simulation, it is updated up to  $T = 2^{17}$  times.

The simulations were conducted in a square domain of size  $L$  with periodic boundary conditions. The position  $\mathbf{r}_i(t)$  of particle  $i$  at time  $t$  evolves according to

$$\mathbf{r}_i(t + \Delta t) = \mathbf{r}_i(t) + \mathbf{v}_i(t)\Delta t, \quad (5)$$

where  $\mathbf{v}_i$  denotes the velocity vector of particle  $i$  with constant speed  $v$  and

$$\mathbf{v}_i(t) = [v \cos(\theta_i(t)), v \sin(\theta_i(t))]. \quad (6)$$

We set the interaction radius  $R = 1, 2, 3, 4, 5$  when investigating the phase transition and set  $v\Delta t = 0.1$  ( $v = 2$ ) which makes the movement of the particles reasonable and gives the particles enough opportunities to interact with each other [16]. By changing other parameters, we create different simulations to satisfy our requirements.

### S2.1 Phase transition with identical influence

All particles in the modified Vicsek model are identical, with uniform interaction strength  $w_{i \rightarrow j} = 1$  for all pairs. The system density is fixed at  $\rho = N/L^2 = 4$ . This density value ( $\rho = 4$ ) was selected because it enables the system to reach an ordered state over time through self-organization [Fig. S2]. Moreover, the noise strength  $\eta$  is systematically varied across the range:

$$\eta \in \{0.05, 0.1, 0.15, \dots, 1.9, 1.95, 2\} \times \pi.$$

By changing  $\eta$ , we change the order of the system. The error bars represent the sample standard deviation calculated from five independent runs.

### S2.2 Pairwise interactions with one-way influence

We set  $R = L$ , so that the influencer is always interacting with followers. Set  $w_{I \rightarrow I} = w_{F \rightarrow F} = 1$ ,  $w_{F \rightarrow I} = 0$  and  $w_{I \rightarrow F} \in \{1, 1.1, 1.2, 1.3, 1.4, 1.5, 1.7, 1.9, 2, 3, 5, 7, 9, 10, 15, 20, 25, 30, 40, 50, 60, 70, 80, 90, 100\}$ . By tuning  $w_{I \rightarrow F}$ , one can change the influence influencer gives to the follower. Moreover, we changed  $\eta$  ( $\eta \in \{0.2, 0.4, 0.6, 0.8, 1.0, 1.2, 1.4, 1.6, 1.8, 2.0\} \times \pi$ ) to change the interaction environment.

### S3. Phase transition and influences

Based on our definition of influence

$$A_{j \rightarrow i}(t) = \frac{w_{j \rightarrow i}[\theta_j(t) - \theta_i(t)]s_{ij}(t)}{\sum_j w_{j \rightarrow i}s_{ij}(t)},$$

different averages can be constructed using the neighbor-average operation  $\langle \cdot \rangle_R$ , the number-average operation  $\langle \cdot \rangle_N$ , the time-average operation  $\overline{\cdot}$ , and the norm operation  $|\cdot|$ . The combination of the above four operations gives 24 types of averages, of which four are unique:

1.  $\overline{\langle |A| \rangle_R \langle \cdot \rangle_N}$ : absolute influences averaged over neighbors, number of particles, and time

$$\overline{\langle |A| \rangle_R \langle \cdot \rangle_N} = \frac{1}{T} \sum_{t=1}^T \frac{1}{N} \sum_{i=1}^N \sum_j |A_{j \rightarrow i}(t)|,$$

2.  $\overline{\langle |A \rangle_R | \rangle_N}$ : absolute neighbor-averaged influences averaged over the number of particles and time:

$$\overline{\langle |A \rangle_R | \rangle_N} = \frac{1}{T} \sum_{t=1}^T \frac{1}{N} \sum_{i=1}^N \left| \sum_j A_{j \rightarrow i}(t) \right|,$$

3.  $\langle \langle |\overline{A}| \rangle_R \rangle_N$ : absolute time-averaged influences averaged over neighbors and the number of particles:

$$\langle \langle |\overline{A}| \rangle_R \rangle_N = \frac{1}{N} \sum_{i=1}^N \sum_j \left| \frac{1}{T} \sum_{t=1}^T A_{j \rightarrow i}(t) \right|,$$

4.  $|\langle \langle \overline{A} \rangle_R \rangle_N|$ : absolute time-averaged, number-averaged, and neighbor-averaged influence:

$$|\langle \langle \overline{A} \rangle_R \rangle_N| = \left| \frac{1}{N} \sum_{i=1}^N \sum_j \frac{1}{T} \sum_{t=1}^T A_{j \rightarrow i}(t) \right|.$$

The main difference among the four unique ones is the position at which the absolute value is taken in the sequence of operations. Their dependences on noise in the modified Vicsek model are shown in Fig. 2(b) and Fig. S3(a)-(c). We note that  $\langle \langle |\overline{A}| \rangle_R \rangle_N$  and  $|\langle \langle \overline{A} \rangle_R \rangle_N|$  are order-of-magnitude smaller than  $\overline{\langle |A| \rangle_R \langle \cdot \rangle_N}$  and  $\overline{\langle |A \rangle_R | \rangle_N}$  because the large number of time steps ( $2^{17}$ ) in our simulations averages out the fluctuations around zero over time. In addition,  $\overline{\langle |A| \rangle_R \langle \cdot \rangle_N} \geq \overline{\langle |A \rangle_R | \rangle_N}$  and  $\langle \langle |\overline{A}| \rangle_R \rangle_N \geq |\langle \langle \overline{A} \rangle_R \rangle_N|$  because  $\sum |a| \geq |\sum a|$  for any real number  $a$ . Indeed, Fig. S3d shows that

$$\overline{\langle |A| \rangle_R \langle \cdot \rangle_N} \geq \overline{\langle |A \rangle_R | \rangle_N} \geq \langle \langle |\overline{A}| \rangle_R \rangle_N \geq |\langle \langle \overline{A} \rangle_R \rangle_N|.$$

Notably,  $\overline{\langle |A \rangle_R | \rangle_N}$  has linear relationships with  $\eta$  when noises are small ( $\eta < \pi$ ). This linear relationship is analyzed as follows.

First, we simplify the expression of  $\langle A \rangle_R$  using  $w_{j \rightarrow i} = 1$ .

$$\langle A_i(t) \rangle_R = \sum_j A_{j \rightarrow i}(t) = \sum_j \frac{w_{j \rightarrow i} F[\theta_j(t) - \theta_i(t)] s_{ij}(t)}{\sum_j w_{j \rightarrow i} s_{ij}(t)} = \sum_j \frac{F[\theta_j(t) - \theta_i(t)] s_{ij}(t)}{\sum_j s_{ij}(t)},$$

Next, in the ordered state, all particles move in the same direction  $\theta_{order}$ . We assume that the neighbors' influences cause a particle to move in the direction  $\theta_{order}$ , which means

$$\theta_{order}(t - \Delta t) = \theta_i(t - \Delta t) + A_i(t - \Delta t).$$

Therefore,

$$\theta_i(t) = F(\theta_i(t - \Delta t) + A_i(t - \Delta t) + \beta_i(t - \Delta t)) = F(\theta_{order}(t - \Delta t) + \beta_i(t - \Delta t)).$$

Similarly,

$$\theta_j(t) = F(\theta_j(t - \Delta t) + A_j(t - \Delta t) + \beta_j(t - \Delta t)) = F(\theta_{order}(t - \Delta t) + \beta_j(t - \Delta t)).$$

Therefore, the differences of  $\theta_i(t)$  and  $\theta_j(t)$  are caused by noise, which equals the differences of  $\beta_i(t - \Delta t)$  and  $\beta_j(t - \Delta t)$ .

$$\langle A_i(t) \rangle_R = \sum_j \frac{F[\theta_j(t) - \theta_i(t)]s_{ij}(t)}{\sum_j s_{ij}(t)} = \sum_j \frac{F[\beta_j(t - \Delta t) - \beta_i(t - \Delta t)]s_{ij}(t)}{\sum_j s_{ij}(t)}.$$

In an ordered state,  $\eta < \pi$ , so  $[\beta_j(t - \Delta t) - \beta_i(t - \Delta t)] \in [-\pi, \pi]$ , which means

$$F[\beta_j(t - \Delta t) - \beta_i(t - \Delta t)] = \beta_j(t - \Delta t) - \beta_i(t - \Delta t).$$

Thus,

$$\langle A_i(t) \rangle_R = \sum_j \frac{[\beta_j(t - \Delta t) - \beta_i(t - \Delta t)]s_{ij}(t)}{\sum_j s_{ij}(t)} = \sum_j \frac{\beta_j(t - \Delta t)s_{ij}(t)}{\sum_j s_{ij}(t)} - \beta_i(t - \Delta t).$$

The first term can be assumed to be zero when there are enough neighbors, i.e., when the density is high enough. Therefore,

$$\langle A_i(t) \rangle_R = -\beta_i(t - \Delta t).$$

Because  $\beta_j(t - \Delta t)$  is uniformly distributed in  $[-\eta/2, \eta/2]$ , its norm  $|\beta_i(t - \Delta t)|$  is uniformly distributed in  $[0, \eta/2]$ . Therefore, the average of  $|\beta_i(t - \Delta t)|$  is  $\eta/4$ :

$$\overline{\langle |A \rangle_R \rangle_N} = \frac{1}{T} \sum_t \frac{1}{N} \sum_i \left| \sum_j A_{j \rightarrow i}(t) \right| = \frac{1}{T} \sum_t \frac{1}{N} \sum_i |\beta_i(t - \Delta t)| = \frac{\eta}{4}.$$

The case for disordered states is more difficult to analyze. Qualitatively, the decrease in  $\overline{\langle |A \rangle_R \rangle_N}$  can be explained as follows. Given angular parameters  $\theta_i(t) \in [0, 2\pi)$  and  $\theta_j(t) \in [0, 2\pi)$ , their difference  $(\theta_j(t) - \theta_i(t)) \in (-2\pi, 2\pi)$ .  $F(\cdot)$  maps this difference to the  $(-\pi, \pi]$  interval. This mapping reduces the value of effective influence, as  $(\theta_j(t) - \theta_i(t))$  often exceeds the  $(-\pi, \pi]$  bounds. Therefore,  $F(\cdot)$  depresses the effect of noises and converts large differences into small differences. This mapping in  $F(\cdot)$  is the reason why  $\overline{\langle |A \rangle_R \rangle_N}$  begins to decrease when  $\eta \geq \pi$ .

The asymptotic value of  $\overline{\langle |A \rangle_R \rangle_N}$  at  $\eta = 2\pi$  can be derived as follows. In

$$\sum_j A_{j \rightarrow i}(t) = \sum_j \frac{F[\theta_j(t) - \theta_i(t)]s_{ij}(t)}{\sum_j s_{ij}(t)},$$

because the noise is at the maximum value  $\eta = 2\pi$ , both  $\theta_j(t)$  and  $\theta_i(t)$  are independently and uniformly distributed over  $[-\pi, \pi]$ . Consequently,  $F[\theta_j(t) - \theta_i(t)]$ , after folding into the range  $[-\pi, \pi]$ , is also uniformly distributed  $[-\pi, \pi]$ . The variance of a uniform distribution over  $[-\pi, \pi]$  is  $\pi^2/3$ , so, according to the Central limit theory (CLT)

$$\langle A \rangle_R = \sum_j A_{j \rightarrow i}(t) \sim \mathcal{N}\left(0, \frac{\pi^2}{3n}\right).$$

Here  $\mathcal{N}(0, \pi^2/3n)$  denotes a Gaussian distribution with mean 0 and variance  $\pi^2/3n$ . Consequently,  $\overline{\langle |A \rangle_R \rangle_N}$  corresponds to the expected absolute value of a Gaussian random variable. Since averaging over  $N$  particles and over time series provide sufficient statistical sampling,  $\overline{\langle |A \rangle_R \rangle_N}$  is the expected value of  $|A \rangle_R$  over a Gaussian distribution  $\mathcal{N}(0, \pi^2/3n)$ .

$$\overline{\langle |A \rangle_R \rangle_N} = \overline{\langle |x \rangle_N} \approx E[|x|] = \int_{-\pi}^{\pi} \frac{|x|}{\sqrt{\frac{2\pi^3}{3n}}} \exp\left(-\frac{x^2}{\frac{2\pi^2}{3n}}\right) dx = \sqrt{\frac{2\pi}{3n}} \approx \sqrt{\frac{2\pi}{3\pi R^2 \rho}} = \sqrt{\frac{2}{3R^2 \rho}}.$$

For  $\rho = 4$  and  $N = 400$ ,  $\overline{\langle |A\rangle_R | \rangle}_N \approx 0.40$  ( $R = 1$ ),  $0.20$  ( $R = 2$ ),  $0.14$  ( $R = 3$ ),  $0.10$  ( $R = 4$ ), and  $0.08$  ( $R = 5$ ) which shows excellent agreement with the simulation result,  $\overline{\langle |A\rangle_R | \rangle}_N \approx 0.39$  ( $R = 1$ ),  $0.20$  ( $R = 2$ ),  $0.14$  ( $R = 3$ ),  $0.10$  ( $R = 4$ ), and  $0.08$  ( $R = 5$ ).

#### S4. Influence and information in pairwise interaction

The time-averaged absolute influence  $\overline{|A_{I \rightarrow F}|}$  increases with  $w_{I \rightarrow F}$  because the norm operation precedes the time averaging operation. Similarly,  $\overline{|A_{I \rightarrow F}|}$  captures the effect of noise in the system and increases with noise strength  $\eta$ . To quantify the above qualitative statements, we derive an analytical expression for  $\overline{|A_{I \rightarrow F}|}$ .

Knowing that

$$A_{I \rightarrow F}(t) = \frac{w_{I \rightarrow F} F(\theta_I(t) - \theta_F(t))}{w_{I \rightarrow F} + w_{F \rightarrow F}}, \theta_I(t) = F(\theta_I(t - \Delta t) + \beta_I(t - \Delta t)),$$

and

$$\theta_F(t) = F(\theta_F(t - \Delta t) + A_{I \rightarrow F}(t - \Delta t) + \beta_F(t - \Delta t)),$$

assume that the follower follows the influencer's direction in the absence of noise at every time step:

$$\theta_I(t - \Delta t) = \theta_F(t - \Delta t) + A_{I \rightarrow F}(t - \Delta t).$$

Therefore, the differences of  $\theta_I(t)$  and  $\theta_F(t)$  are the differences of  $\beta_I(t - \Delta t)$  and  $\beta_F(t - \Delta t)$ :

$$A_{I \rightarrow F}(t) = \frac{w_{I \rightarrow F}}{w_{I \rightarrow F} + w_{F \rightarrow F}} \times F(\beta_I(t - \Delta t) - \beta_F(t - \Delta t)).$$

$\overline{|A_{I \rightarrow F}|}$  is the average value of  $|A_{I \rightarrow F}|$ . As both  $\beta_I(t - \Delta t)$  and  $\beta_F(t - \Delta t)$  are uniformly distributed in  $[-\eta/2, \eta/2]$ ,  $\beta_I(t - \Delta t) - \beta_F(t - \Delta t)$  can be considered as the summation of two independent uniform distributions. Denote  $F(\beta_I(t - \Delta t) - \beta_F(t - \Delta t))$  as a random variable  $Z$ . Then calculating  $\overline{|A_{I \rightarrow F}|}$  is to calculate the average value of  $|Z|$ .

When  $\eta \leq \pi$ ,

$$Z = \beta_I(t - \Delta t) - \beta_F(t - \Delta t),$$

the probability density function of  $Z$  has two parts,

$$p_Z(z) = \begin{cases} \frac{1}{\eta^2}(z + \eta), & -\eta \leq z < 0, \\ \frac{1}{\eta^2}(\eta - z), & 0 \leq z \leq \eta. \end{cases}$$

The probability density function of  $|Z|$  is

$$p_{|Z|}(|z|) = \frac{2}{\eta^2}(\eta - |z|), \quad 0 \leq |z| \leq \eta.$$

Therefore, the average value of  $|A_{I \rightarrow F}|$  when  $\eta \leq \pi$  is

$$\overline{|A_{I \rightarrow F}|} = \frac{w_{I \rightarrow F}}{w_{I \rightarrow F} + w_{F \rightarrow F}} \times \frac{\eta}{3}.$$

When  $\eta > \pi$ ,  $F(\cdot)$  will fold the values of  $(\beta_I(t - \Delta t) - \beta_F(t - \Delta t))$  below  $-\pi$  and above  $+\pi$ , so the probability density function of  $Z$  has four parts,

$$p_Z(z) = \begin{cases} \frac{2}{\eta^2}(\eta - \pi), & -\pi \leq z < -2\pi + \eta, \\ \frac{1}{\eta^2}(z + \eta), & -2\pi + \eta \leq z < 0, \\ \frac{1}{\eta^2}(\eta - z), & 0 \leq z < 2\pi - \eta, \\ \frac{2}{\eta^2}(\eta - \pi), & 2\pi - \eta \leq z \leq \pi. \end{cases}$$

And the probability density function of  $|Z|$  is

$$p_{|z|}(|z|) = \begin{cases} \frac{2}{\eta^2}(\eta - |z|), & 0 \leq |z| < 2\pi - \eta, \\ \frac{4}{\eta^2}(\eta - \pi), & 2\pi - \eta \leq |z| \leq \pi. \end{cases}$$

Therefore,

$$\begin{aligned} \overline{|A_{I \rightarrow F}|} &= \frac{w_{I \rightarrow F}}{w_{I \rightarrow F} + w_{F \rightarrow F}} \times \left( \frac{(2\pi - \eta)^3}{3\eta^2} + \frac{2\pi^2(\eta - \pi)}{\eta^2} \right) \\ &= \frac{w_{I \rightarrow F}}{w_{I \rightarrow F} + w_{F \rightarrow F}} \times \left( \frac{2\pi^3 - 6\pi^2\eta + 6\pi\eta^2 - \eta^3}{3\eta^2} \right). \end{aligned}$$

In conclusion,

$$\overline{|A_{I \rightarrow F}|} = \frac{w_{I \rightarrow F}}{w_{I \rightarrow F} + w_{F \rightarrow F}} \times \begin{cases} \frac{\eta}{3}, & 0 \leq \eta < \pi, \\ \frac{2\pi^3 - 6\pi^2\eta + 6\pi\eta^2 - \eta^3}{3\eta^2}, & \pi \leq \eta \leq 2\pi. \end{cases}$$

## S5. Computation of information-theoretic quantities

The computation of information-theoretic quantities is performed as follows. First, the random variable we choose to do the calculation is the orientation  $\theta$  of the particles because the angular interaction is the only interaction that occurs in the Vicsek model. Moreover, to calculate the information, we discretize the random variables. The binning method we use is equidistant binning, which bins  $\theta$  into 8 bins with equal sizes on the interval  $(-\pi, \pi]$  [17]. For more binning methods, one can refer to [18]. We assume that the interaction satisfies the Markov process. The programs for the calculation of these quantities are all open source. Except for the program to calculate the partial information decomposition with SURD obtained from the work [15], others are from the dit information theory package [19].

In simulating pairwise interaction, we calculate the information flow from the influencer  $I$  to the follower  $F$ . We collect the dataset comprising triples of angular orientations obtained from the simulations

$$\{(\theta_I(t), \theta_F(t), \theta_F(t + \Delta t)) | t \in [0, T)\},$$

and have the joint probabilities,  $p(\theta_I(t), \theta_F(t), \theta_F(t + \Delta t))$ . Then, we can calculate the information flow from the influencer to the follower. For example, the transfer entropy from the influencer to the follower is  $I(\theta_I(t); \theta_F(t + \tau) | \theta_F(t))$  and the unique information from the influencer to the follower is  $Uni(\theta_I(t) \rightarrow \theta_F(t + \tau))$ . The data collection of triples started from 1000th step so that the data correspond to systems' stationary states.

To investigate the information flow in phase transition, we collect pairwise data and construct a distribution that combines all neighbors into one variable and considers the whole time series. The data we collect is

$$\left\{ \left( \theta_j(t), \theta_i(t), \theta_i(t + \Delta t) \right) \middle| \text{for all the } j \text{ s.t. } s_{ij} = 1 \text{ and } j \neq i, \text{ and } t \in [0, T) \right\}.$$

Then, we can have the joint probabilities,  $p(\theta_{nbs}(t), \theta_i(t), \theta_i(t + \Delta t))$ . Here,  $nbs$  means the collection of the neighbors of the particle  $i$  instead of one particular particle. We collapse the neighbors into one variable to represent the environment of the particle  $i$  in order to collect the information of the collective. Then, we can calculate the transfer entropy of the particle  $i$  received from the environment as  $I(\theta_{nbs}(t); \theta_i(t + \tau) | \theta_i(t))$ . For each run, we average the values of the information-theoretic quantities over all particles for  $N = 40$  or one hundred particles for  $N \geq 100$ . The procedure of calculation of other information-theoretic quantities are similar to the calculation of transfer entropy. Notably, the data points in the region  $\eta < 0.3\pi$  have large error bars. Because we chose eight bins, and each bin spans  $\pi/4$ , the positions of bin edges affect the discretized probability distribution significantly in the low-noise region.

Supplementary figures

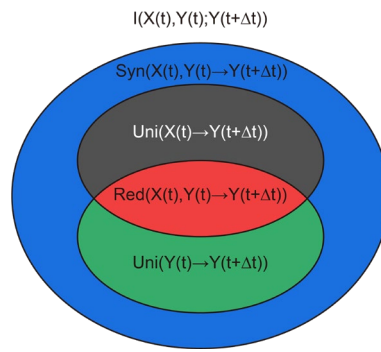


FIG. S1. The structure of partial information decomposition in pairwise interaction between  $X$  and  $Y$ .

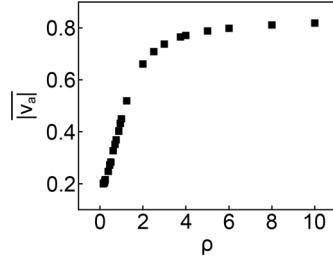


FIG. S2. The dependence of  $\overline{|v_a|}$  density  $\rho$  with  $L = 20$  and constant noise  $\eta = 2.0 \approx 0.64\pi$ .

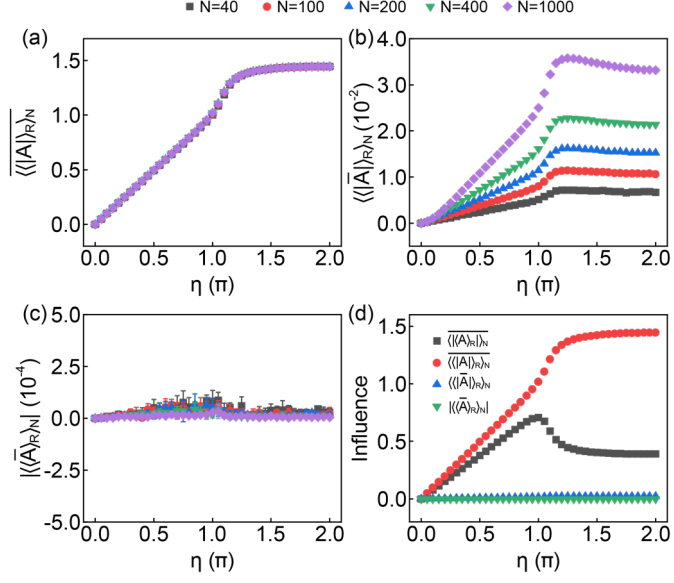


FIG. S3. The performance of the constructed order parameters versus noises  $\eta$  (in the unit of  $\pi$  rad). (a) Dependence of  $\langle\langle |A| \rangle_R \rangle_N$  on  $\eta$ . (b) Dependence of  $\langle\langle \bar{A} \rangle_R \rangle_N$  on  $\eta$ . (c) Dependence of  $|\langle\langle \bar{A} \rangle_R \rangle_N|$  on  $\eta$ . (d) The performance of these four order parameters with  $N = 400$ .

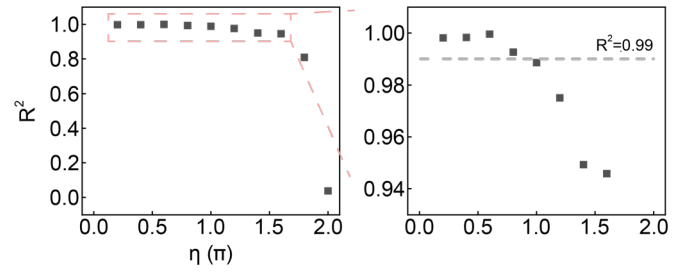


FIG. S4. The  $R^2$  (coefficient of determination) of the linear fittings of Fig. 2(e).

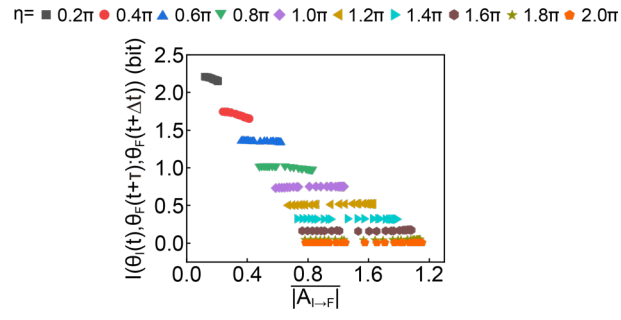


FIG. S5.  $I(\theta_I(t), \theta_F(t); \theta_F(t + \Delta t))$  versus  $|A_{I \rightarrow F}|$ . Each color represents one noise strength. The weights vary from 1 to 100. Symbols of the same color represent different weights of the same noise strength.

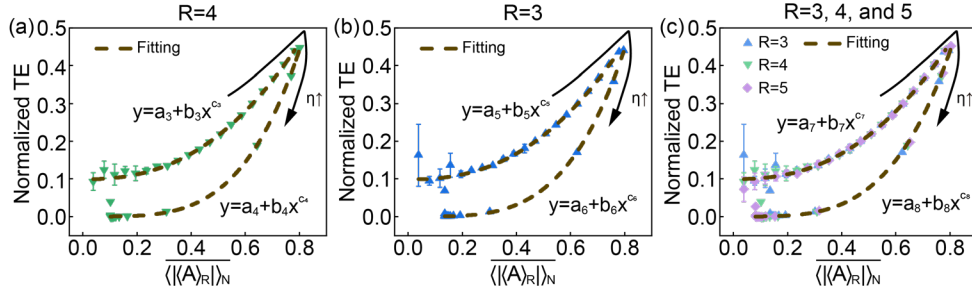


FIG. S6. Normalized TE versus  $\overline{\langle(A)_R\rangle_N}$  for different values of  $R$  at  $\rho = 4$  and  $N=400$ . (a) For  $R = 4$ ,  $a_3 = 0.099 \pm 0.002$ ,  $b_3 = 0.618 \pm 0.002$ ,  $c_3 = 2.409 \pm 0.027$ ,  $a_4 = 0$ ,  $b_4 = 1.049 \pm 0.115$ , and  $c_4 = 3.880 \pm 0.287$ . (b) For  $R = 3$ ,  $a_5 = 0.099 \pm 0.002$ ,  $b_5 = 0.619 \pm 0.003$ ,  $c_5 = 2.406 \pm 0.034$ ,  $a_6 = 0$ ,  $b_6 = 1.048 \pm 0.094$ , and  $c_6 = 3.835 \pm 0.177$ . (c) For  $R = 3, 4$ , and  $5$  data combined,  $a_7 = 0.099 \pm 0.001$ ,  $b_7 = 0.616 \pm 0.001$ ,  $c_7 = 2.404 \pm 0.016$ ,  $a_8 = 0$ ,  $b_8 = 1.007 \pm 0.048$ , and  $c_8 = 3.730 \pm 0.057$ .

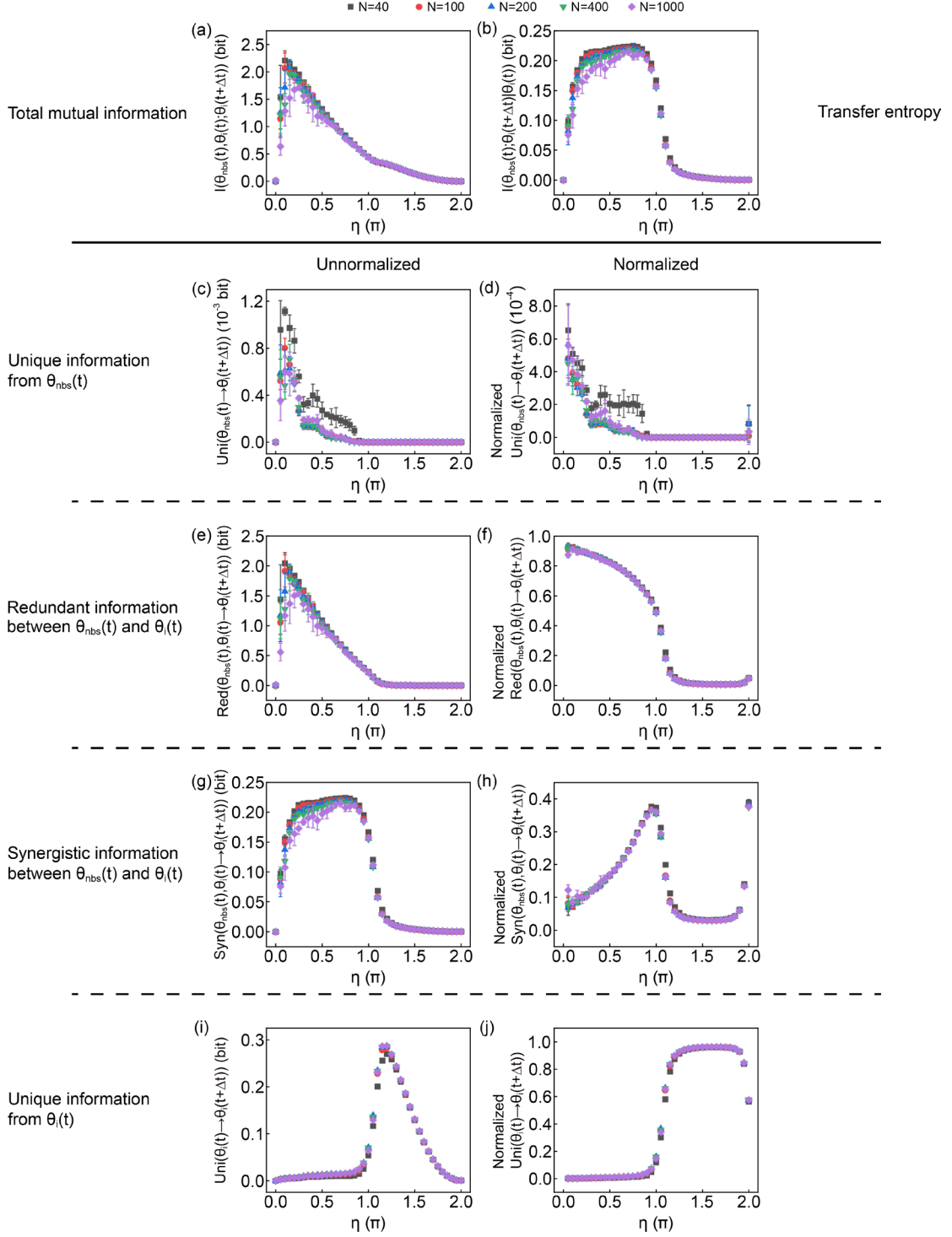


FIG. S7. AMI partial information decomposition method at  $R = 1$ . (a) The total mutual information  $I(\theta_{nbs}(t), \theta_i(t); \theta_i(t + \Delta t))$  versus  $\eta$ . (b) The TE  $I(\theta_{nbs}(t); \theta_i(t + \Delta t) | \theta_i(t))$  versus  $\eta$ . (c)  $Uni(\theta_{nbs}(t) \rightarrow \theta_i(t + \Delta t))$  versus  $\eta$ . (d) Normalized  $Uni(\theta_{nbs}(t) \rightarrow \theta_i(t + \Delta t))$  versus  $\eta$ . (e)  $Red(\theta_{nbs}(t), \theta_i(t) \rightarrow \theta_i(t + \Delta t))$  versus  $\eta$ . (f) Normalized  $Red(\theta_{nbs}(t), \theta_i(t) \rightarrow \theta_i(t + \Delta t))$  versus  $\eta$ . (g)  $Syn(\theta_{nbs}(t), \theta_i(t) \rightarrow \theta_i(t + \Delta t))$  versus  $\eta$ . (h) Normalized  $Syn(\theta_{nbs}(t), \theta_i(t) \rightarrow \theta_i(t + \Delta t))$  versus  $\eta$ . (i)  $Uni(\theta_i(t) \rightarrow \theta_i(t + \Delta t))$  versus  $\eta$ . (j) Normalized  $Uni(\theta_i(t) \rightarrow \theta_i(t + \Delta t))$  versus  $\eta$ .

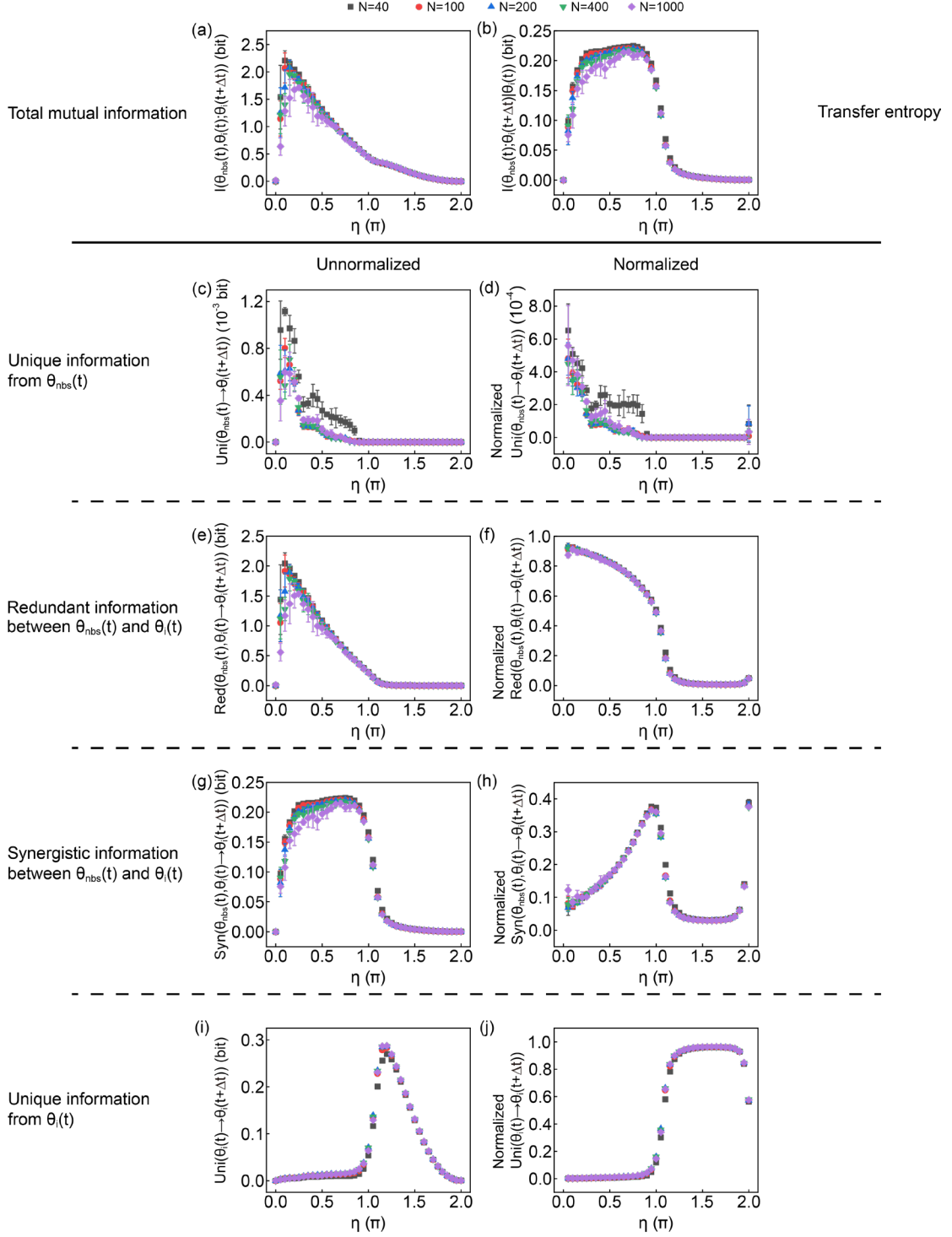


FIG. S8. SURD partial information decomposition method at  $R = 1$ . (a) The total mutual information  $I(\theta_{nbs}(t), \theta_i(t); \theta_i(t + \Delta t))$  versus  $\eta$ . (b) The TE  $I(\theta_{nbs}(t); \theta_i(t + \Delta t) | \theta_i(t))$  versus  $\eta$ . (c)  $Uni(\theta_{nbs}(t) \rightarrow \theta_i(t + \Delta t))$  versus  $\eta$ . (d) Normalized  $Uni(\theta_{nbs}(t) \rightarrow \theta_i(t + \Delta t))$  versus  $\eta$ . (e)  $Red(\theta_{nbs}(t), \theta_i(t) \rightarrow \theta_i(t + \Delta t))$  versus  $\eta$ . (f) Normalized  $Red(\theta_{nbs}(t), \theta_i(t) \rightarrow \theta_i(t + \Delta t))$  versus  $\eta$ . (g)  $Syn(\theta_{nbs}(t), \theta_i(t) \rightarrow \theta_i(t + \Delta t))$  versus  $\eta$ . (h) Normalized  $Syn(\theta_{nbs}(t), \theta_i(t) \rightarrow \theta_i(t + \Delta t))$  versus  $\eta$ . (i)  $Uni(\theta_i(t) \rightarrow \theta_i(t + \Delta t))$  versus  $\eta$ . (j) Normalized  $Uni(\theta_i(t) \rightarrow \theta_i(t + \Delta t))$  versus  $\eta$ .

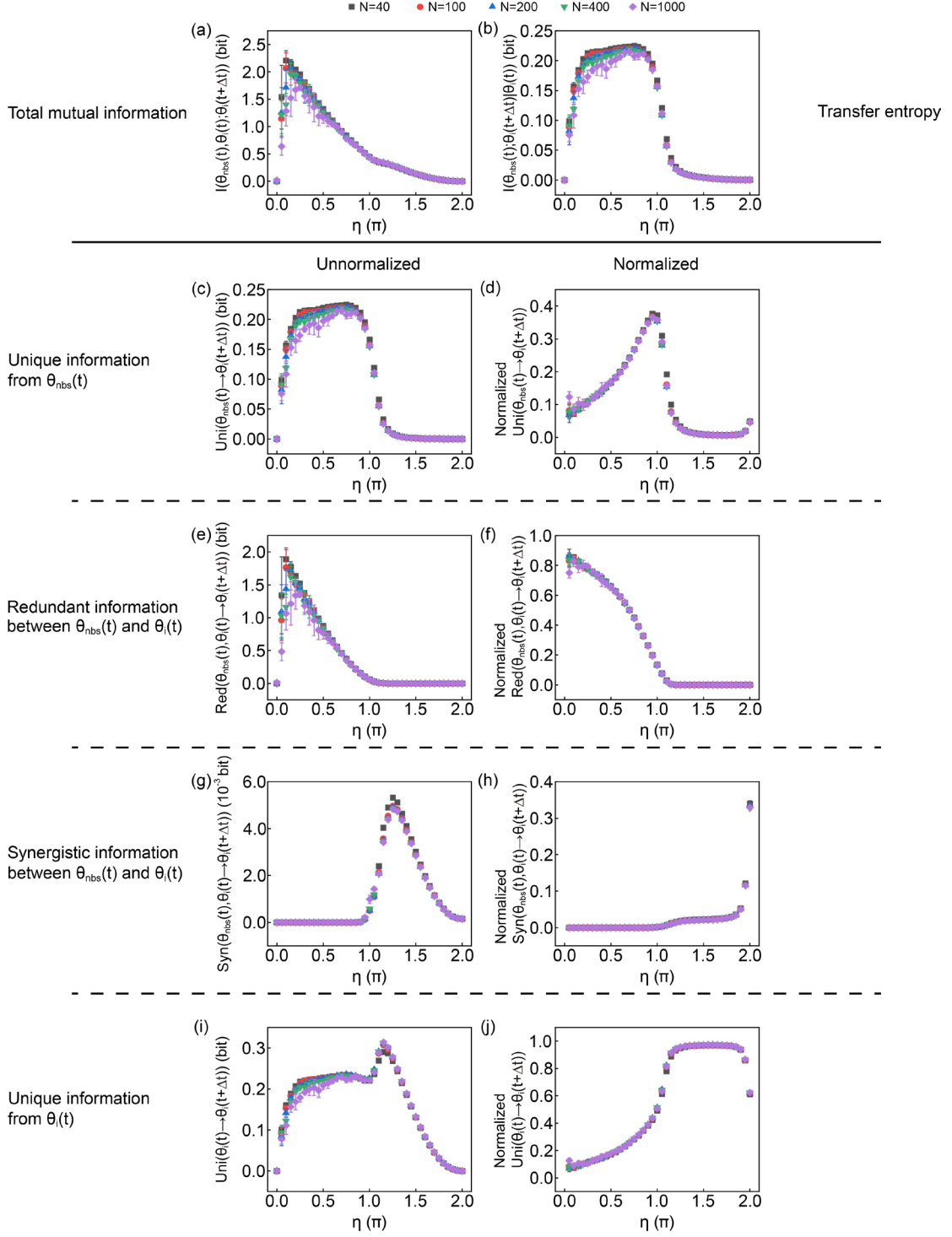


FIG. S9. IMI partial information decomposition method at  $R = 1$ . (a) The total mutual information  $I(\theta_{nbs}(t), \theta_i(t); \theta_i(t + \Delta t))$  versus  $\eta$ . (b) The TE  $I(\theta_{nbs}(t); \theta_i(t + \Delta t) | \theta_i(t))$  versus  $\eta$ . (c)  $Uni(\theta_{nbs}(t) \rightarrow \theta_i(t + \Delta t))$  versus  $\eta$ . (d) Normalized  $Uni(\theta_{nbs}(t) \rightarrow \theta_i(t + \Delta t))$  versus  $\eta$ . (e)  $Red(\theta_{nbs}(t), \theta_i(t) \rightarrow \theta_i(t + \Delta t))$  versus  $\eta$ . (f) Normalized  $Red(\theta_{nbs}(t), \theta_i(t) \rightarrow \theta_i(t + \Delta t))$  versus  $\eta$ . (g)  $Syn(\theta_{nbs}(t), \theta_i(t) \rightarrow \theta_i(t + \Delta t))$  versus  $\eta$ . (h) Normalized  $Syn(\theta_{nbs}(t), \theta_i(t) \rightarrow \theta_i(t + \Delta t))$  versus  $\eta$ . (i)  $Uni(\theta_i(t) \rightarrow \theta_i(t + \Delta t))$  versus  $\eta$ . (j) Normalized  $Uni(\theta_i(t) \rightarrow \theta_i(t + \Delta t))$  versus  $\eta$ .

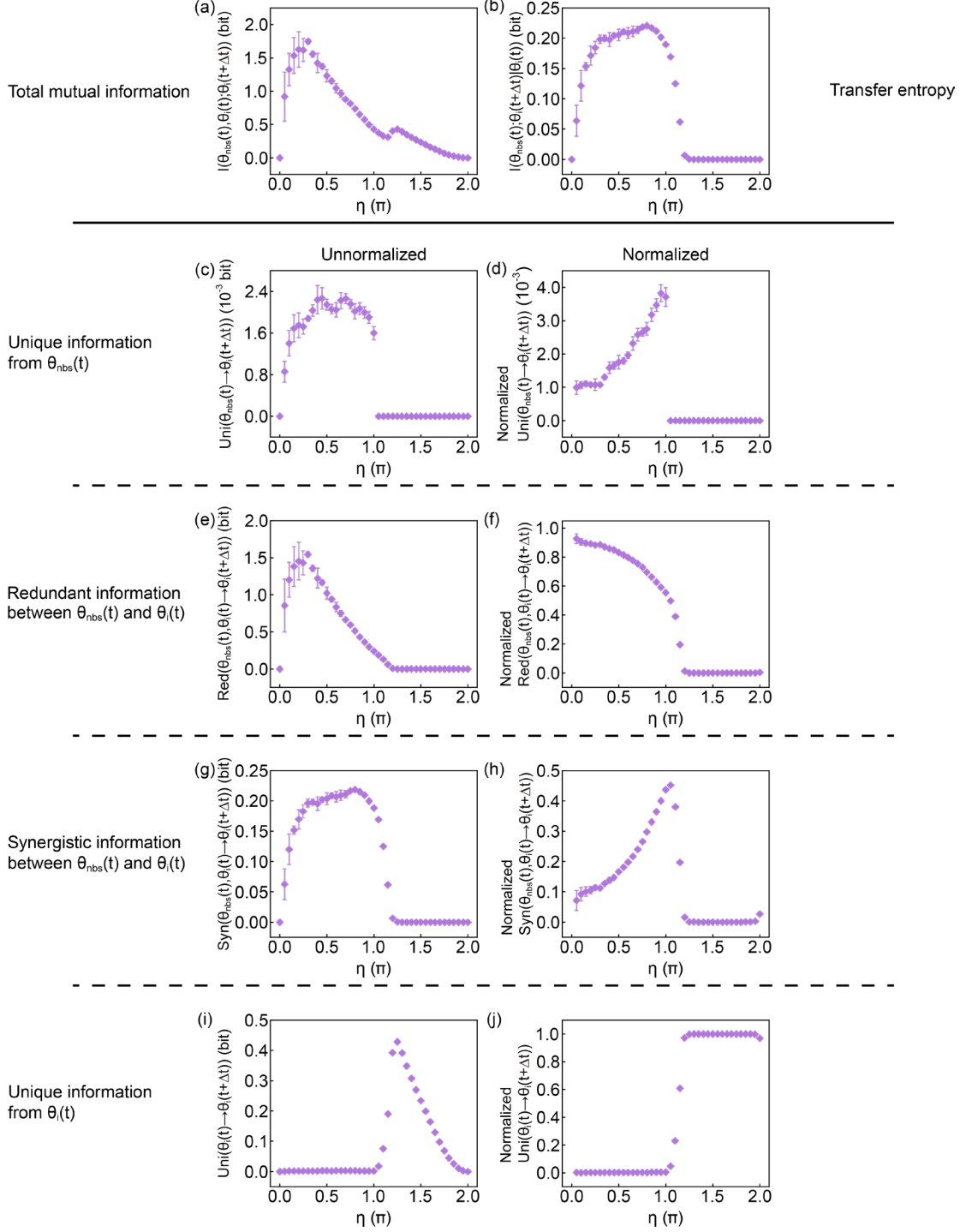


FIG. S10. AMI partial information decomposition method at  $R = 5$  and  $N = 400$ . (a) The total mutual information  $I(\theta_{nbs}(t), \theta_i(t); \theta_i(t + \Delta t))$  versus  $\eta$ . (b) The TE  $I(\theta_{nbs}(t); \theta_i(t + \Delta t) | \theta_i(t))$  versus  $\eta$ . (c)  $Uni(\theta_{nbs}(t) \rightarrow \theta_i(t + \Delta t))$  versus  $\eta$ . (d) Normalized  $Uni(\theta_{nbs}(t) \rightarrow \theta_i(t + \Delta t))$  versus  $\eta$ . (e)  $Red(\theta_{nbs}(t), \theta_i(t) \rightarrow \theta_i(t + \Delta t))$  versus  $\eta$ . (f) Normalized  $Red(\theta_{nbs}(t), \theta_i(t) \rightarrow \theta_i(t + \Delta t))$  versus  $\eta$ . (g)  $Syn(\theta_{nbs}(t), \theta_i(t) \rightarrow \theta_i(t + \Delta t))$  versus  $\eta$ . (h) Normalized  $Syn(\theta_{nbs}(t), \theta_i(t) \rightarrow \theta_i(t + \Delta t))$  versus  $\eta$ . (i)  $Uni(\theta_i(t) \rightarrow \theta_i(t + \Delta t))$  versus  $\eta$ . (j) Normalized  $Uni(\theta_i(t) \rightarrow \theta_i(t + \Delta t))$  versus  $\eta$ .

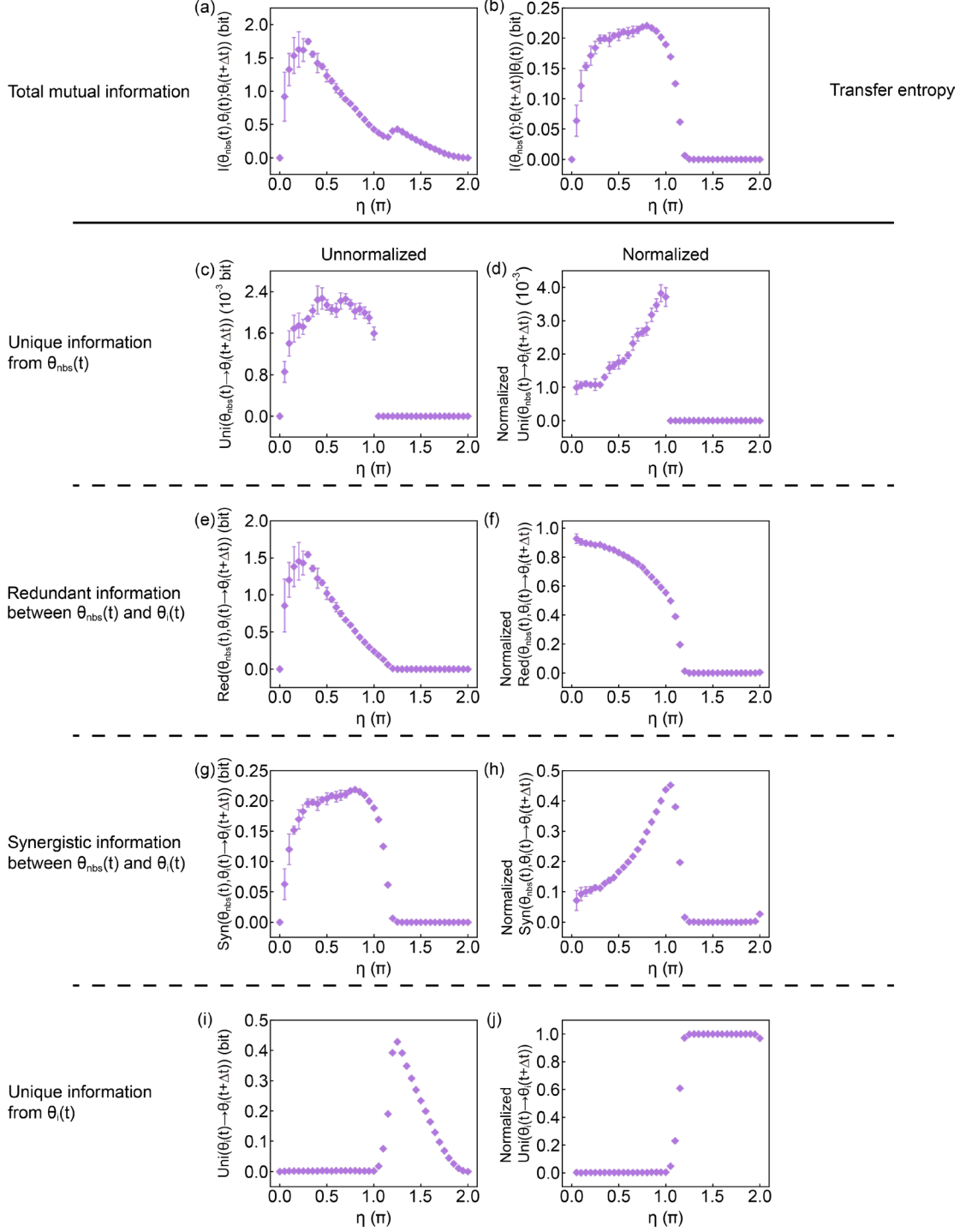


FIG. S11. SURD partial information decomposition method at  $R = 5$  and  $N = 400$ . (a) The total mutual information  $I(\theta_{nbs}(t), \theta_i(t); \theta_i(t + \Delta t))$  versus  $\eta$ . (b) The TE  $I(\theta_{nbs}(t); \theta_i(t + \Delta t) | \theta_i(t))$  versus  $\eta$ . (c)  $Uni(\theta_{nbs}(t) \rightarrow \theta_i(t + \Delta t))$  versus  $\eta$ . (d) Normalized  $Uni(\theta_{nbs}(t) \rightarrow \theta_i(t + \Delta t))$  versus  $\eta$ . (e)  $Red(\theta_{nbs}(t), \theta_i(t) \rightarrow \theta_i(t + \Delta t))$  versus  $\eta$ . (f) Normalized  $Red(\theta_{nbs}(t), \theta_i(t) \rightarrow \theta_i(t + \Delta t))$  versus  $\eta$ . (g)  $Syn(\theta_{nbs}(t), \theta_i(t) \rightarrow \theta_i(t + \Delta t))$  versus  $\eta$ . (h) Normalized  $Syn(\theta_{nbs}(t), \theta_i(t) \rightarrow \theta_i(t + \Delta t))$  versus  $\eta$ . (i)  $Uni(\theta_i(t) \rightarrow \theta_i(t + \Delta t))$  versus  $\eta$ . (j) Normalized  $Uni(\theta_i(t) \rightarrow \theta_i(t + \Delta t))$  versus  $\eta$ .

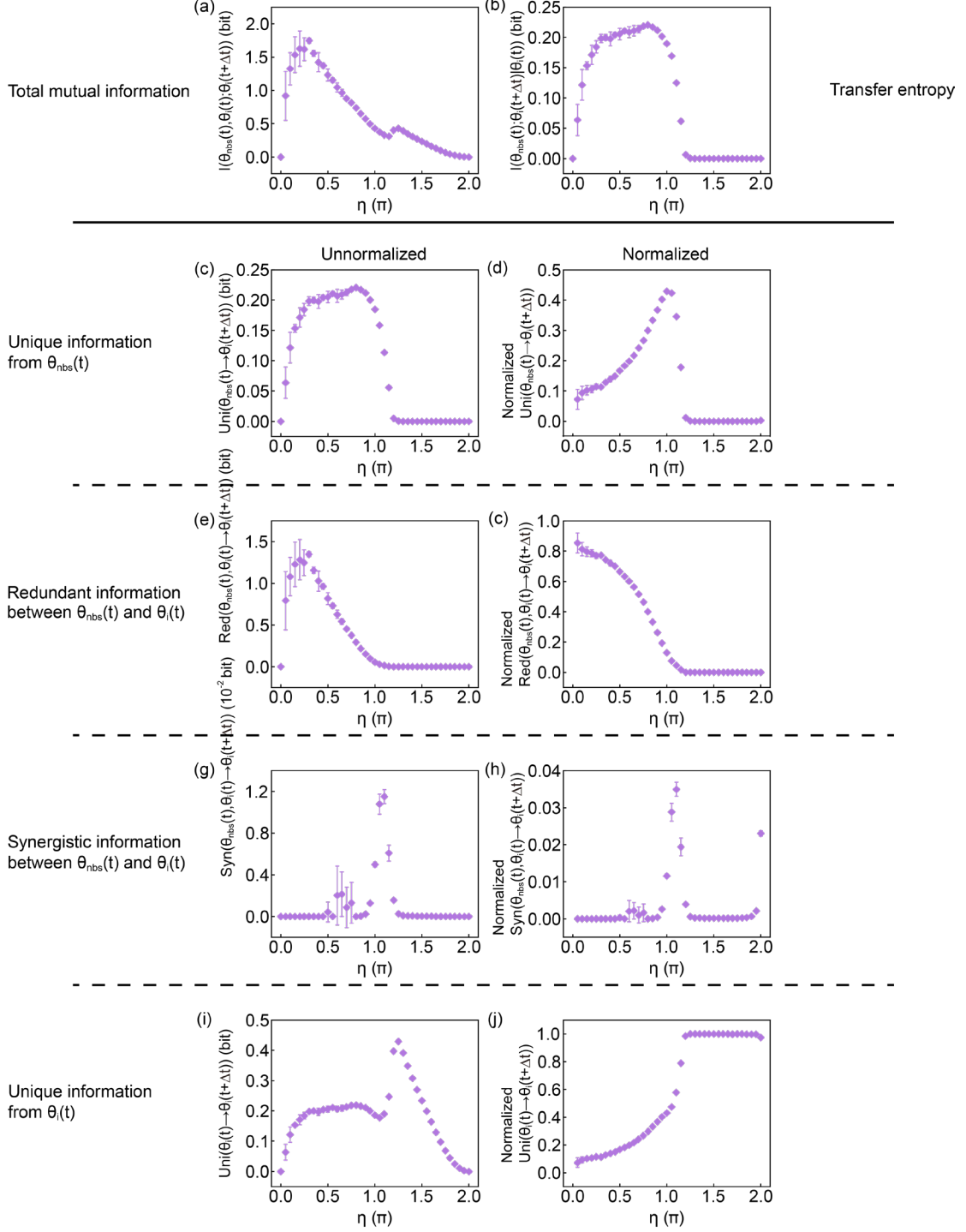


FIG. S12. IMI partial information decomposition method at  $R = 5$  and  $N = 400$ . (a) The total mutual information  $I(\theta_{nbs}(t), \theta_i(t); \theta_i(t + \Delta t))$  versus  $\eta$ . (b) The TE  $I(\theta_{nbs}(t); \theta_i(t + \Delta t) | \theta_i(t))$  versus  $\eta$ . (c)  $Uni(\theta_{nbs}(t) \rightarrow \theta_i(t + \Delta t))$  versus  $\eta$ . (d) Normalized  $Uni(\theta_{nbs}(t) \rightarrow \theta_i(t + \Delta t))$  versus  $\eta$ . (e)  $Red(\theta_{nbs}(t), \theta_i(t) \rightarrow \theta_i(t + \Delta t))$  versus  $\eta$ . (f) Normalized  $Red(\theta_{nbs}(t), \theta_i(t) \rightarrow \theta_i(t + \Delta t))$  versus  $\eta$ . (g)  $Syn(\theta_{nbs}(t), \theta_i(t) \rightarrow \theta_i(t + \Delta t))$  versus  $\eta$ . (h) Normalized  $Syn(\theta_{nbs}(t), \theta_i(t) \rightarrow \theta_i(t + \Delta t))$  versus  $\eta$ . (i)  $Uni(\theta_i(t) \rightarrow \theta_i(t + \Delta t))$  versus  $\eta$ . (j) Normalized  $Uni(\theta_i(t) \rightarrow \theta_i(t + \Delta t))$  versus  $\eta$ .

## SI Reference

- [1] T. Schreiber, Measuring Information Transfer, *Phys. Rev. Lett.* **85**, 461 (2000).
- [2] J. F. Ramirez-Villegas, M. Besserve, Y. Murayama, H. C. Evrard, A. Oeltermann, and N. K. Logothetis, Coupling of hippocampal theta and ripples with pontogeniculooccipital waves, *Nature* **589**, 96 (2021).
- [3] U. S. Basak, M. E. Islam, and S. Sattari, Inferring interaction domains of collectively moving agents with varying radius of influence, *AIP Advances* **13**, 035312 (2023).
- [4] K. Takamizawa and M. Kawasaki, Transfer entropy for synchronized behavior estimation of interpersonal relationships in human communication: identifying leaders or followers, *Sci Rep* **9**, 10960 (2019).
- [5] U. S. Basak, S. Sattari, M. Hossain, K. Horikawa, and T. Komatsuzaki, Transfer entropy dependent on distance among agents in quantifying leader-follower relationships, *Biophysics. Physicobiol.* **18**, 131 (2021).
- [6] R. G. James, B. D. M. Ayala, B. Zakirov, and J. P. Crutchfield, *Modes of Information Flow*, arXiv:1808.06723.
- [7] P. L. Williams and R. D. Beer, *Nonnegative Decomposition of Multivariate Information*, arXiv:1004.2515.
- [8] M. Harder, C. Salge, and D. Polani, Bivariate measure of redundant information, *Phys. Rev. E* **87**, 012130 (2013).
- [9] N. Bertschinger, J. Rauh, E. Olbrich, J. Jost, and N. Ay, Quantifying Unique Information, *Entropy* **16**, 4 (2014).
- [10] V. Griffith and C. Koch, *Quantifying Synergistic Mutual Information*, arXiv:1205.4265.
- [11] R. A. A. Ince, Measuring Multivariate Redundant Information with Pointwise Common Change in Surprisal, *Entropy* **19**, 7 (2017).
- [12] R. G. James, J. Emenheiser, and J. P. Crutchfield, Unique information via dependency constraints, *J. Phys. A: Math. Theor.* **52**, 014002 (2018).
- [13] R. G. James, J. Emenheiser, and J. P. Crutchfield, Unique Information and Secret Key Agreement, *Entropy* **21**, 1 (2019).
- [14] S. Sattari, U. S. Basak, R. G. James, L. W. Perrin, J. P. Crutchfield, and T. Komatsuzaki, Modes of information flow in collective cohesion, *Sci. Adv.* **8**, eabj1720 (2022).
- [15] Á. Martínez-Sánchez, G. Arranz, and A. Lozano-Durán, Decomposing causality into its synergistic, unique, and redundant components, *Nat. Commun.* **15**, 9296 (2024).
- [16] T. Vicsek, A. Czirók, E. Ben-Jacob, I. Cohen, and O. Shochet, Novel Type of Phase Transition in a System of Self-Driven Particles, *Phys. Rev. Lett.* **75**, 1226 (1995).
- [17] U. S. Basak, S. Sattari, K. Horikawa, and T. Komatsuzaki, Inferring domain of interactions among particles from ensemble of trajectories, *Phys. Rev. E* **102**, 012404 (2020).
- [18] *Phys. Rev. E* **77**, 026214 (2008) - *Inferring the Directionality of Coupling with Conditional Mutual Information*, <https://journals.aps.org/pre/abstract/10.1103/PhysRevE.77.026214>.
- [19] R. G. James, C. J. Ellison, and J. P. Crutchfield, dit: a Python package for discrete information theory, *JOSS* **3**, 738 (2018).